An application for polymeric foams

Hilbeth P. Azikri de Deus
IF-SC - Santa Catarina Federal Institute of Education, Science and Technology, Joinville Campus, Department of Metal Mechanics, Joinville/SC – Brazil
Marcelo Krajnc Alves
UFSC - Federal University of Santa Catarina, Trindade Campus, Department of Mechanical Engineering, Florianópolis/SC – Brazil

Abstract

This work proposes a material model and algorithms for applications in polymeric foams. The constitutive relationship is given in association of work-conjugate pair Hencky strain deformation measure and rotated Kirchhoff stress tensor are proposed and explored. The viscoplastic model applied for polymeric foam is non associative, based on a modified von Mises model (by inclusion of the hydrostatic pressure) and incorporates a non linear isotropic hardening law. A regularization approach is proposed to guarantee that the relative density evolution is into the factible set $K\rho$. Various examples are presented along this work aiming to atest the models and implemented algorithms. The problem is formulated within a Total Lagrangian descripton. The Galerkin finite element method is used for numerical approach. Finally some problem cases are solved, and the proposed model, the robustness and performance of the algorithms employed are tested.

Keywords: polymeric foam, Kirchhoff stress tensor, Hencky strain tensor, viscoplasticity.

1 Introduction

Polymeric foams are widely used in industry and in domestic applications. These foams have a high energy absorption capacity, are useful for shock applications, acoustic and thermal insulating problems. For these reasons, they are used in aircraft and automotive industry, buildings and packaging. Combining good mechanical properties with low density, rigid polymer foams can also be used as structural materials.

The polymeric foams are made of a skeleton composed of open or closed cells, which represent the basic unit of these materials. The mechanical response of polymeric foams depend on the cells geometric characteristics, such as cell wall thickness, shape and size distributions, and on the intrinsic properties of the polymer in the cell wall. In order to model such complex materials, different constitutive relations have been proposed in the literature and are basically divided into two groups: complex

Mechanics of Solids in Brazil 2009, H.S. da Costa Mattos & Marcílio Alves (Editors)
Brazilian Society of Mechanical Sciences and Engineering, ISBN 978-85-85769-43-7

modeling approaches that proposes constitutive relation which describe the average behavior of the foam [1–5] or simpler models that try to represent the cells as an assemblage of structural elements (geometrically periodic cells) [6–9] and relate to analytically elastic material properties and yield stress to the foam relative density.

In order to properly use these materials, one must understand their microstructure/macroscopic mechanical property relationships. Indeed, the mechanical response of these materials depends on their geometrical characteristics, and on the intrinsic properties of the polymer in the cell wall. The geometrical characteristics are determined by the cell wall thickness, the size distribution and the cells shape.

In this work we consider a complex modeling approach and propose a hyperelastic-viscoplastic constitutive relation for modeling the behavior of open cell foam materials. Moreover, based on experimental results, we consider the hyperelastic response to depend on the relative density of the material [10, 11].

Among the various proposed constitutive relations, one can cite the power-law model, described in Chaboche and Rousselier [12], that is generally accepted to give good predictions for low strain rates. However, as the strain rate increases, such a model is unable to describe the observed decreasing strain rate dependence. Also, in the limit, with the increase of the strain rate, the model should be capable to account for a saturation of the material response, as observed experimentally. With the aim of incorporating this material behavior in a unified viscoplastic model, other propositions for the flow rule have been used in the literature. Examples include a hyperbolic sine function, see [13], an exponential function or the addition of a second power-law function to the flow law, as proposed by Chaboche [14]. Some models even combine plasticity with viscoplasticity in order to achieve these goals, as seen in Almroth *et al* [15]. Here, we make use of the constitutive equation proposed by Benallal, see [16], which can be applied for large strain rates and account for the saturation of the overstress where the strain rate is very high.

The proposed model is implemented in a Total Lagrangian framework that considers: a multiplicative decomposition of the deformation gradient, into a plastic and an elastic part and a constitutive relation given in terms of the logarithmic, or Hencky, strain measure and the rotated Kirchhoff stress. The advantage of choosing this conjugate stress-strain pair in the formulation of the constitutive relation is that it leads to a return mapping whose form is the same as the one derived in the small deformation plasticity framework. In addition, one consider the temperature to be low and the deformation rate to be sufficiently high in order to consider the existence of an elastic response and a yield function.

2 Theoretical approach

This paper proposes an elastoviscoplastic constitutive relation for the finite deformation of isotropic crushable polymeric foams, which incorporates the phenomena of creep, relaxation and deformation rate sensitivity in the response of the material.

The model considers the material to have a hardening behavior that is characterized by two curves: one for the compaction response and one for the uniaxial compressive test, which must be determined experimentally. In addition, as a result of experimental observation, the model incorporates a different

Mechanics of Solids in Brazil 2009, H.S. da Costa Mattos & Marcílio Alves (Editors)
Brazilian Society of Mechanical Sciences and Engineering, ISBN 978-85-85769-43-7

response in compression and tension and assumes the hyperelastic behavior to depend on the relative density of the material. In compression the ability of the material to deform volumetrically is enhanced by cell wall buckling processes as described by Gibson & Ashby [6] and Girson et al. [7].

It is assumed that the foam cell deformation is not recoverable instantaneously and can be seen as being viscoplastic. Under tension loading, the cell walls break readily so the tensile load bearing capacity of crushable foams may be considerably smaller than its compressive load bearing capacity.

3 Kinetics of deformation

The plasticity model presented in this paper considers the multiplicative decomposition of the deformation gradient F into an elastic part, F^e, and a viscoplastic part, F^{vp}, as illustrated in Fig. 1. Thus,

$$F = F^e F^{vp} \tag{1}$$

with $F = \nabla\phi(x_o, t)$, where ϕ is the deformation function.

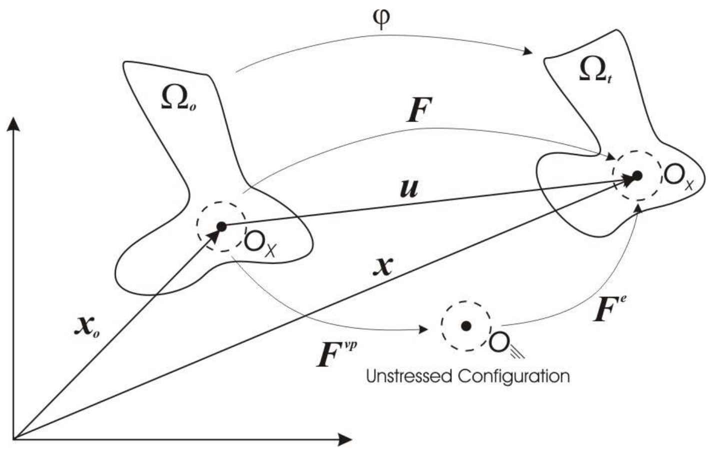

Figure 1: Kinematics of deformation.

However, since $F^e = R^e U^e$, $F^{vp} = R^{vp} U^{vp}$, $U^e = \sqrt{C^e} = \sqrt{F^{eT} F^e}$, $L^e = \dot{F}^e (F^e)^{-1}$, $L^{vp} = F^e \dot{F}^{vp} (F^{vp})^{-1} (F^e)^{-1}$ and $D = sym(L) = D^e + D^{vp}$, the deformation measure, given in terms of the logarithmic strain tensor, may be expressed as

$$\begin{aligned} E^e(x_o, t) &= \frac{1}{2} \ln \left(C^e(x_o, t) \right); \\ &= \ln \left(U^e(x_o, t) \right). \end{aligned} \tag{2}$$

Brazilian Society of Mechanical Sciences and Engineering, ISBN 978-85-85769-43-7

Hill [17] pointed out that the stress-strain pairs must be such that the rate of work density remains preserved. The enforcement of this criterion together with the assumption of an isotropic response of the material leads to the identification of the conjugate stress measure, which is given by the rotated Kirchhoff stress,

$$\bar{\tau} = R^T \tau \, R \tag{3}$$

where τ is the Kirchhoff stress, $\tau = \det(F)\,\sigma$, with σ denoting the Cauchy stress [18, 19].

4 The Yield surface definition

To define the yield function, we introduce the following basic definitions:

- The deviatoric rotated Kirchhoff stress, given by:

$$\bar{\tau}^D = \bar{\tau} - \frac{1}{3} tr(\bar{\tau})\, I \tag{4}$$

- The von Mises effective rotated Kirchhoff stress, given by

$$q = \sqrt{\frac{3}{2} \bar{\tau}^D : \bar{\tau}^D} \tag{5}$$

- The hydrostatic pressure stress, given by

$$p = -\frac{1}{3} tr(\bar{\tau}^D) \tag{6}$$

Thus, from Eq. (4) and Eq.(6) we may express the rotated Kirchhoff stress as $\bar{\tau} = \bar{\tau}^D - p\,I$. Here, we consider the yield function for crushable foam materials, shown in Fig. 3, to be defined in terms of the Kirchhoff stress measure and given by

$$\tilde{\Im}(p, q, \bar{\varepsilon}_k) = \sqrt{q^2 + [\alpha(\bar{\varepsilon}_k)]^2 [p - p_o(\bar{\varepsilon}_k)]^2} - B(\bar{\varepsilon}_k) \tag{7}$$

in which $\alpha = \alpha(\bar{\varepsilon}_k)$ and $p_o = p_o(\bar{\varepsilon}_k)$ are functions of the internal variables $\bar{\varepsilon}_k$. The parameters o p_o and B of the yield ellipse are related to the yield strength in hydrostatic compression, p_c, and to the yield strength in hydrostatic tension, p_t, by

$$p_o = \frac{1}{2}(p_c - p_t), \;\; B = \alpha A = \alpha \frac{p_t + p_c}{2} \tag{8}$$

where p_c and p_t are positive numbers and A is the length of the (horizontal) p-axis of the yield ellipse (see Fig. 2 and Fig. 3).

The evolution of the yield ellipse is controlled by the volumetric compacting viscoplastic strain,

$$\bar{\varepsilon}_1 = \bar{\varepsilon}_v^{vp} = -\ln(J^{vp}), \;\; J^{vp} = \det(F^{vp}) \tag{9}$$

employed in the volumetric hardening model, and by the axial viscoplastic strain,

$$\bar{\varepsilon}_2 = \bar{\varepsilon}_a^{vp} = -\ln\left(\frac{L_f}{L_o}\right) \tag{10}$$

defined in a unilateral compression test, in which L_f is the unloaded length of the specimen, after the deformation has been applied, and L_o is the length of the initial configuration of the reference specimen. To define the hardening behavior, some experimental test data must be obtained, which comprise:

- A uniaxial compression test data
- A hydrostatic compression test data

These hardening curves must be experimentally evaluated and incorporated to the model. Here, we assume the hydrostatic tension strength, p_t , to be proportional to the hydrostatic compression strength, i.e.,

$$p_t = \alpha_p p_c \tag{11}$$

for some constant value $\alpha_p \in [5\%, 10\%]$, see Hanssen *et al* [20] and Hallquist [1]. In addition, we assume the hydrostatic compression strength, p_c , to evolve as a result of compaction (increase in density) or dilation (reduction in density) of the material, i.e.

$$p_c = p_c^o + H_p(\bar{\varepsilon}_v^{vp}) \tag{12}$$

where p_c^o is the initial hydrostatic compression yield strength and $H_p(\bar{\varepsilon}_v^{vp})$ is the hydrostatic compression strength hardening law, given in terms of the volumetric compacting viscoplastic strain.

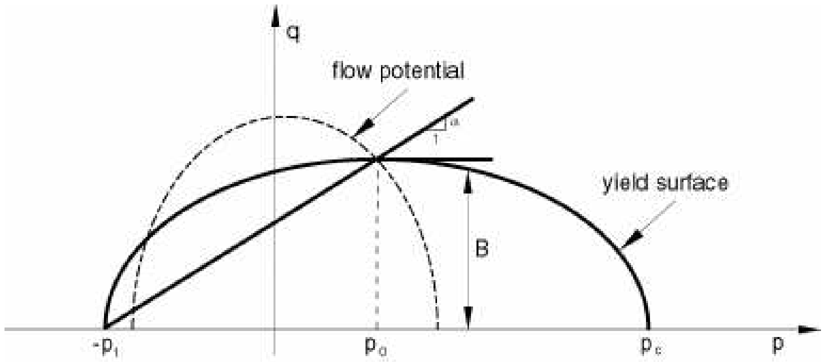

Figure 2: Yield surface.

In order to compute $\alpha(\bar{\varepsilon}_v^{vp};\bar{\varepsilon}_a^{vp})$ different independent experimental test is required. Here, we employ a uniaxial compression tests. Notice that, different tests could also have been considered. Now, since the type of impact loading that we want to simulate is dominated by a uniaxial compression type of loading, the best result for the analysis may be probably obtained by using a uniaxial compression test. From a uniaxial compression test we obtain

$$\bar{\sigma}_c(\bar{\varepsilon}_a^{vp}) = \bar{\sigma}_c^o + H(\bar{\varepsilon}_a^{vp}) \tag{13}$$

where $\bar{\sigma}_c^o$ is the initial yield stress, $H(\bar{\varepsilon}_a^{vp})$ is the strain hardening function and $\bar{\varepsilon}_a^{vp}$ is the equivalent viscoplastic strain. Now in a general 3D case, the axial viscoplastic strain is not well defined. However, the uniaxial test response may be incorporated indirectly by using the uniaxial relation

$$\bar{\varepsilon}_a^{vp} = \frac{\bar{\varepsilon}_c^{vp}}{(1-2\nu_p)} \tag{14}$$

Now, using (Eq.11-14), we can compute $\alpha(\bar{\varepsilon}_v^{vp};\bar{\varepsilon}_a^{vp})$, as follows

$$\alpha(\bar{\varepsilon}_v^{vp};\bar{\varepsilon}_a^{vp}) = \frac{\bar{\sigma}_c}{\left[p_c p_t - \frac{1}{3}\bar{\sigma}_c\left(p_c - p_t\right) - \frac{1}{9}\bar{\sigma}_c^2\right]^{\frac{1}{2}}} \tag{15}$$

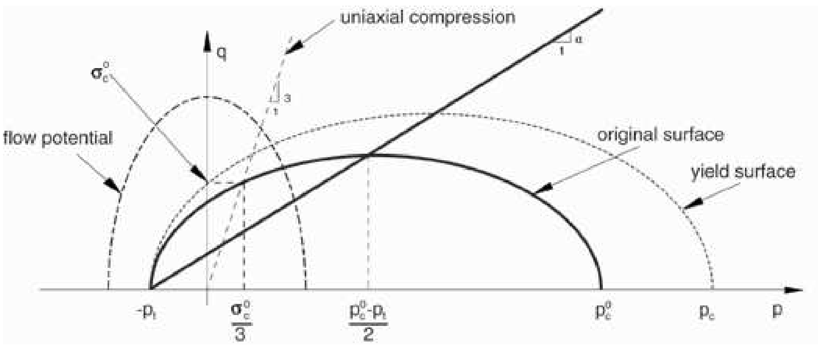

Figure 3: Volumetric hardening.

5 The non-associative viscoplastic flow potential

The viscoplastic strain rate for the volumetric hardening model is assumed to be given by

$$\bar{D}^{vp} = \dot{\lambda}\frac{\partial G}{\partial \bar{\tau}} \tag{16}$$

complemented by postulating a null viscoplastic spin, compatible with viscoplastic isotropy, i.e., $\bar{W}^{vp} = 0$ (null second order tensor). Here, $\dot{\lambda}$ is the viscoplastic multiplier which must satisfy: $\dot{\lambda} \geqslant 0$, which is given by a constitutive relation. The evolution of the viscoplastic deformation is computed as

Brazilian Society of Mechanical Sciences and Engineering, ISBN 978-85-85769-43-7

$$\dot{F}^{vp} = \overset{vp}{\breve{D}} F^{vp} \tag{17}$$

where $\overset{vp}{\breve{L}} = (F^e)^{-1} L^{vp} F^e$ (unstressed local configuration) and $\overset{vp}{\breve{W}} = (U^e)^{-1} W^{vp} U^e = 0$ (null second order tensor). The viscoplastic flow potential (see Fig. 3) for this model is given by

$$G(p, q) = \sqrt{q^2 + \beta^2 p^2} \tag{18}$$

in which β is related to the plastic Poisson's ratio ν_p by

$$\beta = \frac{3}{\sqrt{2}} \sqrt{\frac{1 - 2\nu_p}{1 + \nu_p}} \tag{19}$$

The usual assumption, for polymeric foams is to consider p $\nu = 0.0$. In the absence of the knowledge of the plastic Poisson's ratio, the consideration of a zero plastic Poisson's ratio is a reasonable assumption, as shown in Zhang *et al* [4], Gibson & Ashby [6] and Gilchrist & Mills [21].

6 Evolution law for the accumulated viscoplastic strain

In the case of viscoplastic materials, the viscoplastic multiplier λ is computed by solving a constitutive evolution equation. Here, we make use Benallal's model, see Lemaitre [16] for more details, given by

$$\dot{\bar{e}}^{vp} = \ln \left[\left(1 - \frac{\tilde{\Im}(p, q, \bar{\varepsilon}_k)}{K_v} \right)^{-M} \right] \tag{20}$$

where

$$\dot{\bar{e}}^{vp} = \left[\frac{2}{3} \left(\bar{D}^{vp} : \bar{D}^{vp} \right) \right]^{\frac{1}{2}} \tag{21}$$

Notice that, the evolution of the accumulated viscoplastic strain, which enables the determination of the viscoplastic multiplier, is based on a model that accounts for a saturation of the material response to the increase of the applied rate of deformation. In fact, we have that

$$\tilde{\Im}(p, q, \bar{\varepsilon}_k) = \sigma^v \geqslant 0 \tag{22}$$

where we denote σ v as the over stress measure, we obtain

$$\sigma^v = K_v \left[1 - \exp \left(\frac{\dot{\bar{e}}}{M} \right)^{-M} \right] \tag{23}$$

7 Hyperelastic response

Here, we consider the elastic response to be given, in terms of the logarithmic or Hencky strain tensor and therotated Kirchhoff stress, as

$$\bar{\tau} = 2\mu(\rho^*)E^e + \left[\kappa(\rho^*) - \frac{2}{3}\mu(\rho^*)\right] tr(E^e)\, I \tag{24}$$

where

$$\begin{aligned} \mu(\rho^*) &= \frac{E(\rho^*)}{2\,(1+\nu_o)}; \\ \kappa(\rho^*) &= \frac{E(\rho^*)}{3\,(1-2\nu_o)}, \end{aligned} \tag{25}$$

In which $E(\rho^*)$, is the Young modulus, I is the second order identity, tensor, $\kappa(\rho^*)$ is the bulk modulus, $\mu(\rho^*)$ is the Lamé's coefficient or the shear modulus and ρ^* denoting the relative density, which is defined by the ratio of the foam density, ρ , with the fully compact material density, ρ_M , i.e.,

$$\rho^* = \frac{\rho}{\rho_M} \tag{26}$$

The continuity equation may be written in terms of the relative density as

$$\rho_o^* = \det(F)\rho^* \tag{27}$$

in which $\rho_o^* = \rho_o^*(x_o)$ denotes the initial relative density, defined in the reference configuration, and $\rho^* = \rho^*(x_o, t)$ the actual relative density, defined at the reference configuration. Here, it's important to notice that the set of physical allowable relative densities, related to physical admissible deformation processes, is given by $K = \{\rho^* |\, 0 < \rho^* \leqslant 1\}$.

In order to impose implicitly these constraints, we will rewrite the Young modulus as

$$E(\rho^*) = [c(\rho^*)^\gamma + I_K(\rho^*)]\, E_M \tag{28}$$

where $I_K(\rho^*)$ represents the indicator set of K, i.e.,

$$I_K(\rho^*) = \begin{cases} 0, \ if\ \rho^* \in K_\rho; \\ \infty, \ if\ \rho^* \notin K_\rho. \end{cases} \tag{29}$$

This expression may be regularized by using a combined internal and external penalty approaches, i.e., we consider a differentiable function $\Psi_\eta(\rho^*)$ such that

$$I_K(\rho^*) = \lim_{\eta \to 0} [\Psi_\eta(\rho^*)] \tag{30}$$

Based on the above results, we consider the following constitutive relations

$$\Psi_\eta(\rho^*) = \eta\frac{1}{\rho^*} + \frac{1}{\eta}\left[\langle\rho^* - 1\rangle^+\right]^2 \tag{31}$$

and

$$E(\rho^*) = \left\{c(\rho^*)^\gamma + \eta\frac{1}{\rho^*} + \frac{1}{\eta}\left[\langle\rho^* - 1\rangle^+\right]\right\} E_M \tag{32}$$

with E_M representing the Young's modulus of the fully dense material respectively and η a penalty parameter.

8 Total Lagrangean formulation – weak form

The approach used here is the total Lagragean formulation. Considering the reference configuration Ω_o, defined at t_o, a bounded domain with a Lipschitz boundary $\partial\Omega_o$ subjected to a body force b defined on Ω_o, a prescribed surface traction defined on Γ_o^t and a prescribed displacement defined on Γ_o^u, where $\partial\Omega_o = \overline{\Gamma_o^t \cup \Gamma_o^u}$ and $\Gamma_o^t \cap \Gamma_o^u$.

Taking the motion function $\phi_t : \Re^3 \to \Re^3$ such that $x = \phi(x_o, t) = \phi_t(x_o) \;\therefore\; x_o = \phi_t^{-1}(x)$. It follows that the displacement field is defined as: $x = u(x_o, t) + x_o \;\therefore\; u_o(x_o, t) = \phi_t(x_o) - x_o = x - x_o = x - \phi_t^{-1}(x) = u(x_o, t)$. Thus, it is possible to announce the problem in the reference configuration as:

Problem 2 For each $t \in [0, t_f]$ determine $u_o(x_o, t)$ that solves the following boundary value problem stated as

$$div\, P(x_o, t) + \rho_o(x_o)\, b(x_o, t) = 0 \quad in \quad \Omega_o \tag{33}$$

$$P(x_o, t)\, n_o(x_o, t) = \bar{t}_o(x_o, t) \qquad in \quad \Gamma_o^t \tag{34}$$

$$u_o(x_o, t) = \bar{u}_o(x_o) \qquad in \quad \Gamma_o^u \tag{35}$$

with $b(x_o, t) \in L_2(\Omega_o)$ and $\bar{u}_o(x_o) \in H_{00}^{1/2}(\Gamma_o^u)$ for each $t \in [0, t_f]$.

Let us define now the following sets, for each time $t \in [0, t_f]$

$$Kin_o^u = \left\{u_o : \Omega_o \to \Re^3 \left| u_o \in H^1(\Omega_o),\, u_o(x_o, t) = \bar{u}_o(x_o) \; in\; \Gamma_o^u \right.\right\} \tag{36}$$

$$Var_o^u = \left\{\hat{v} : \Omega_o \to \Re^3 \left| \hat{v} \in H^1(\Omega_o),\, \hat{v}(x_o) = 0 \; in\; \Gamma_o^u \right.\right\} \tag{37}$$

Thus it has the weak form of the problem

Problem 3 For each $t \in [0, t_f]$ determine $u_o(x_o, t) \in Kin_o^u$ such that

$$\int_{\Omega_o} P : \nabla\hat{v}\, d\Omega_o = \int_{\Omega_o} \rho_o b \cdot \hat{v}\, d\Omega_o + \int_{\Gamma_o^t} \bar{t}_o \cdot \hat{v}\, d\partial\Omega_o, \;\forall\hat{v} \in Var_o^u \tag{38}$$

For each $t \in [0, t_f]$, it can denoting

$$\Im\left(u_o;\hat{v}\right)=\int_{\Omega_o}P:\nabla\hat{v}\,d\Omega_o-\int_{\Omega_o}\rho_o b\cdot\hat{v}\,d\Omega_o\;-\int_{\Gamma_o^t}\bar{t}_o\cdot\hat{v}\,d\partial\Omega_o,\;\forall\hat{v}\in Var_o^u \tag{39}$$

Then, the problem can be stated as

Problem 4 For each $t\in[0,t_f]$ determine $u_o(x_o,t)\in Kin_o^u$ such that

$$\Im\left(u_o;\hat{v}\right)=0,\;\forall\hat{v}\in Var_o^u \tag{40}$$

The problem above is approached by Newton method in association with Galerkin-FEM, and the incremental formulation follows from the schematic algorithm in Tab. 1

Table 1: Newton's method algorithm – incremental formulation.

For each time step $t=t_n$;
(i) Initialize the iteration counter $k\leftarrow 0$;
(ii) Initialize the variable vector $u_{n+1}^0=u_n$;
(iii) Compute the *residue vector*, $error=\Vert residue\ vector\Vert$;
(iv) Do while ($error>tolerance^1$)
(1) Determine the tangent modulus $\left[\aleph(u_{n+1}^k)\right]_{ijkl}=\left.\frac{\partial P_{ij}}{\partial F_{kl}}\right\vert_{u=u_{n+1}^k}$
(2) Solve the problem $\int_{\Omega_o}\aleph(u_{n+1}^k)\nabla(\Delta u_{n+1}^k)\,:\nabla\hat{v}d\Omega_o=-\Im\left(u_{n+1_o}^k;\hat{v}\right),\;\forall\hat{v}\in Var_o^u$;
(3) Actualize the variable vector $u_{n+1}^{k+1}=u_{n+1}^k+\Delta u_{n+1}^k$;
(4) Compute the new $error$;
(5) Actualize $\Im\left(u_{n+1}^k;\hat{v}\right)\leftarrow\Im\left(u_{n+1}^{k+1};\hat{v}\right)$ and $k\leftarrow k+1$;
End Do while.

$^{(1)}$: previously defined.

9 Numerical examples

For these applications, one used a mesh with two six points triangular elements. The developed code is written in Fortran 90 and for post processing, it's used the GID 8.0 software. The global tolerance is 10-6.

EXAMPLE 1: Here, the simulation of a uniaxial compression test is presented. The specimen consists of a cylindrical bar with a radius R=28mm and a height of 50mm. The material parameters used in this analysis are described in Table 2. The process consists is prescribing the displacement of the upper part of the specimen, with a total upsetting of $\bar{u} = -30\,mm$, applied in order to compress the body. Due to the axisymmetry condition, only half of the domain is modeled. Fig. 4 shows the displacement field, in the y-direction.

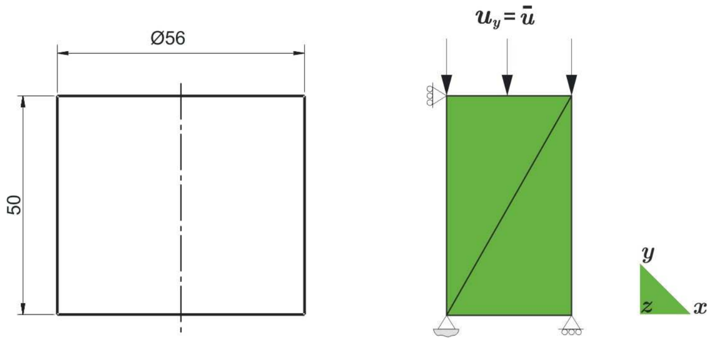

Figure 4: Compression test.

Table 2: Material Parameters[(1)].

$E_M = 928,09288\,MPa$	$\nu_p = 0,0$	$c = 0,3$
$\sigma_y^o = 0,10582\,MPa$	$\rho_o^* = 0,049\,MPa$	$M = 4,0$
$p_c^o = 0,04047\,MPa$	$\nu = 0,25$	$K_v = 0,005$
$\alpha_p = 0,1$	$\gamma = 1,54$	$\eta = 10^{-5}$

(1) see Zhang *et al* [4], Gibson & Ashby [6] and Gilchrist & Mills [21]

In next figures (see Fig. 5 and Fig. 6), one presents the time evolution of σ_{yy} in the body (constant profile along entire body) for two different rates. One can observe the evolution of stress σ_{yy} component in the observation time. Note that the numerical results shows good agreement to the experimental solution of the problem for load time step [4, 6, 21].

Mechanics of Solids in Brazil 2009, H.S. da Costa Mattos & Marcílio Alves (Editors)
Brazilian Society of Mechanical Sciences and Engineering, ISBN 978-85-85769-43-7

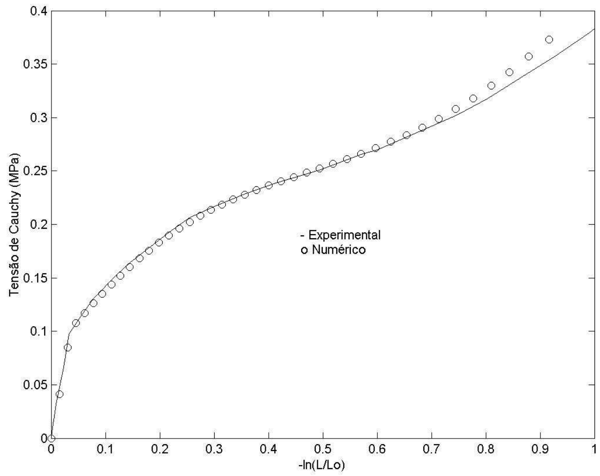

Figure 5: Compression test (0,0016 s^{-1}).

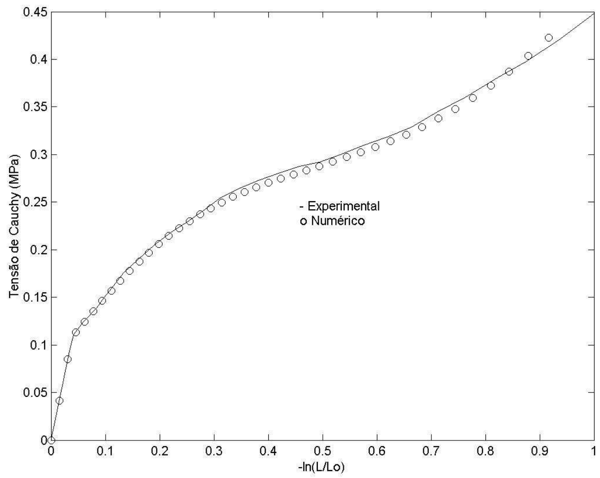

Figure 6: Compression test (0,08 s^{-1}).

At the final observation instant, we get the following results: $\bar{\varepsilon}_v^{vp} = \bar{\varepsilon}_a^{vp} = 0,90196$ (rate 0,0016 s^{-1}), $\bar{\varepsilon}_v^{vp} = \bar{\varepsilon}_a^{vp} = 0,90058$ (rate 0,08 s^{-1}), $\rho^* = 0,1216$ (rates 0,0016 s^{-1} and 0,08 s^{-1}) (constant profile along entire body – see Fig. 7).

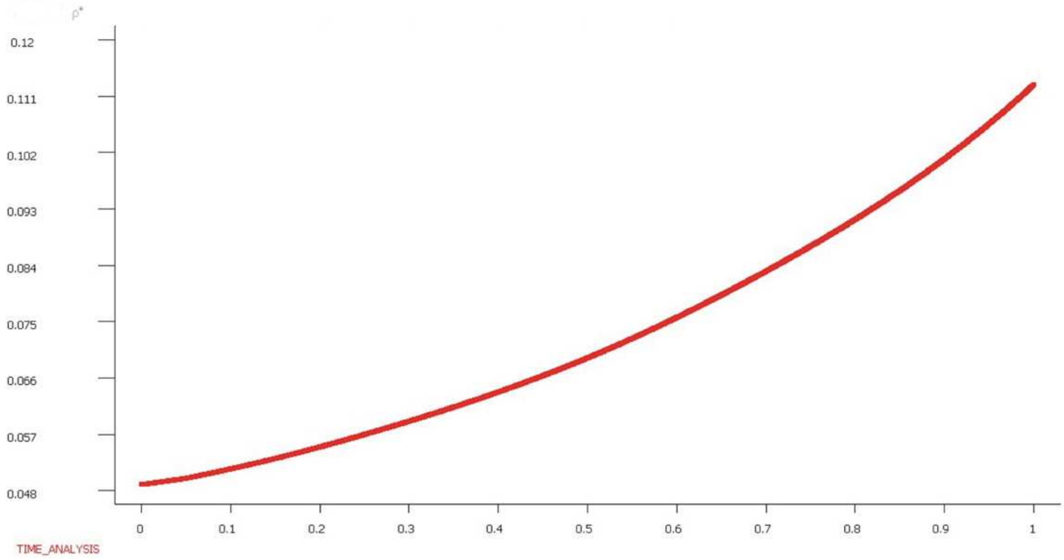

Figure 7: Relative density evolution.

EXAMPLE 2: This example considers an axisymmetric problem that consists of the upsetting of a conical slab, whose dimensions are: r1=90mm; r2=45mm and h=100mm. The analysis consists of prescribing the displacement of the upper wall, with a total upsetting of $\bar{u} = -50\,mm$, as shown in Fig. 8, and employs an integration mesh with 240 isoparametric tri-6 elements. Due to the axisymmetry condition, only half of the domain is modeled. Fig. 9 shows the displacement field, in the y-direction at the final observation instant (rates 0,0016 s^{-1} and 0,08 s^{-1}).

The Fig. 10 shows the Cauchy stress component σ_{xx} profile (rate 0,08 s^{-1}), Fig. 11 shows the Cauchy stress component σ_{xx} profile (rate 0,0016 s^{-1}),. Fig. 12 shows the Cauchy stress component σ_{xy} profile (rate 0,08 s^{-1}), Fig. 13 shows the Cauchy stress component σ_{xy} profile (rate 0,0016 s^{-1}), Fig. 14 shows the Cauchy stress component σ_{yy} profile (rate 0,08 s^{-1}), Fig. 15 shows the Cauchy stress component σ_{yy} profile (rate 0,0016 s^{-1}), Fig. 16 shows the relative density ρ^* profile (rates 0,08 s^{-1} and 0,0016 s^{-1}), and the Fig. 17 and Fig.18 show the equivalent von Misses stress profile for rates 0,08 s^{-1} and 0,0016 s^{-1}.

The evolutions of the Cauchy Stress versus the logarithm strain and of the relative density versus the volumetric plastic strain are shown in Figure 10, at points A and B. Point A is at the left upper edge and B at the right upper edge of the mesh depicted in Figure 8. The sub indexes 1 and 2 refer to the solution obtained by using the FE and EFG methods respectively.

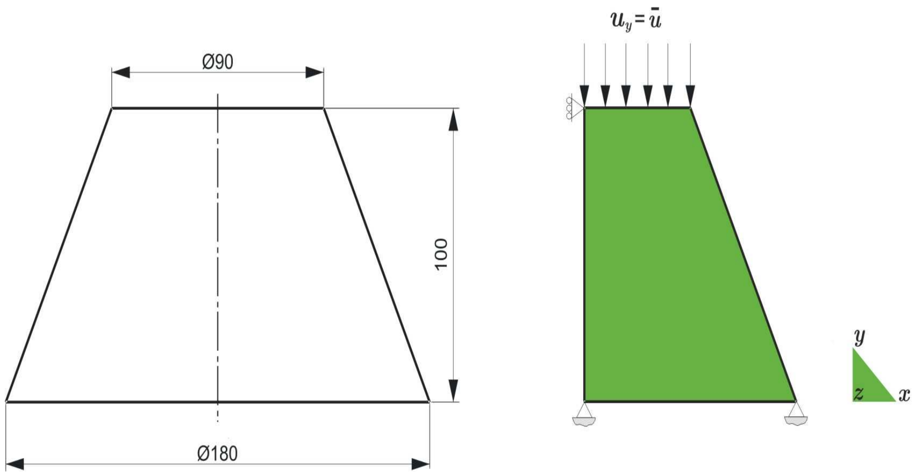

Figure 8: Conical slab.

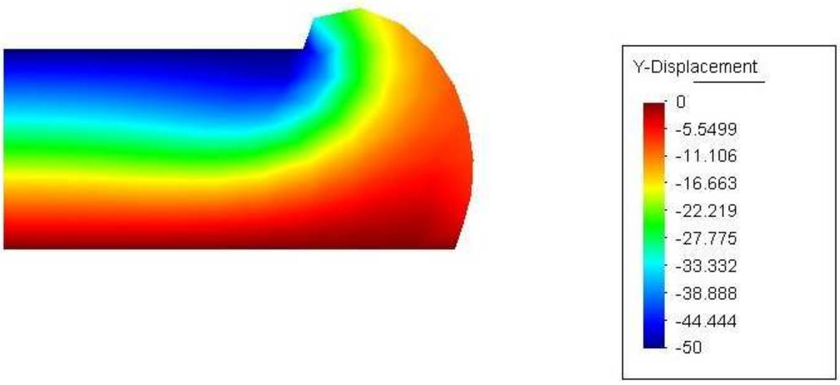

Figure 9: Y-displacement (mm).

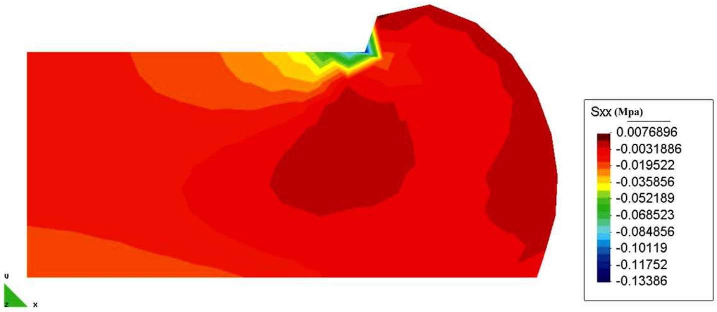

Figure 10: σ_{xx} profile (0,08s^{-1}).

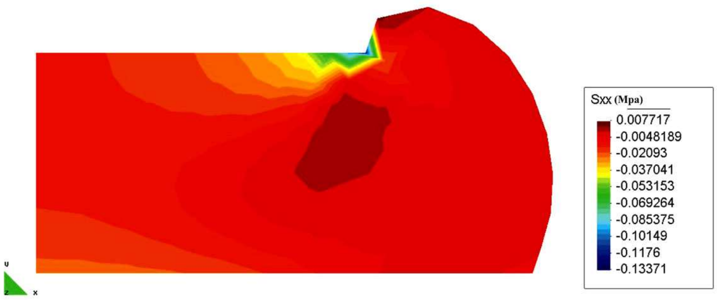

Figure 11: σ_{xx} profile (0,0016s^{-1}).

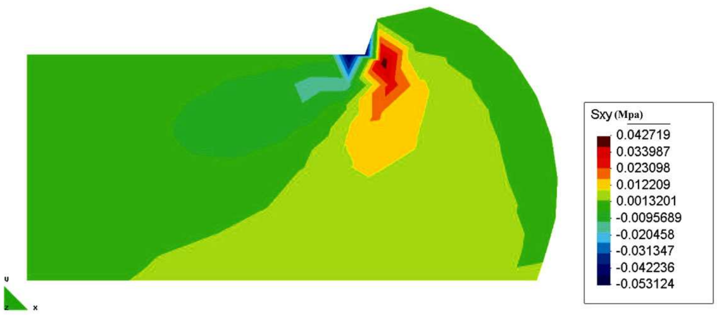

Figure 12: σ_{xy} profile (0,08s^{-1}).

Mechanics of Solids in Brazil 2009, H.S. da Costa Mattos & Marcílio Alves (Editors)
Brazilian Society of Mechanical Sciences and Engineering, ISBN 978-85-85769-43-7

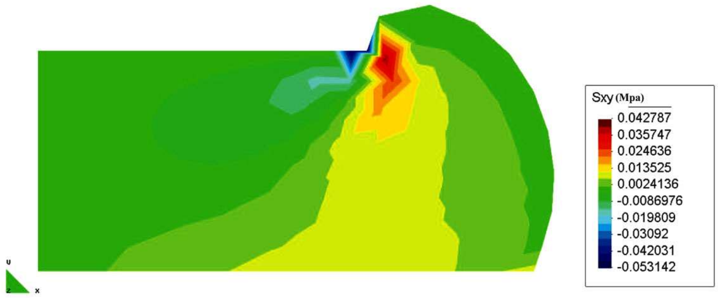

Figure 13: σ_{xy} profile (0,0016s^{-1}).

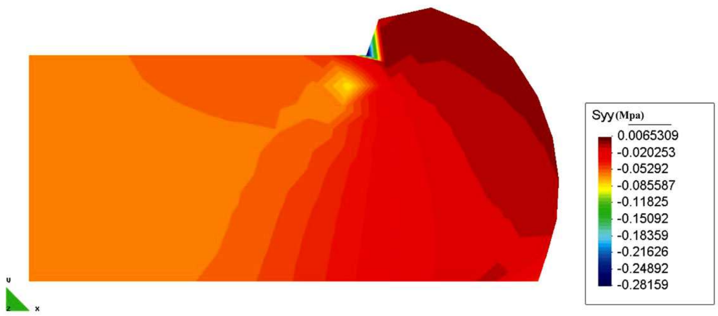

Figure 14: σ_{yy} profile (0,08s^{-1}).

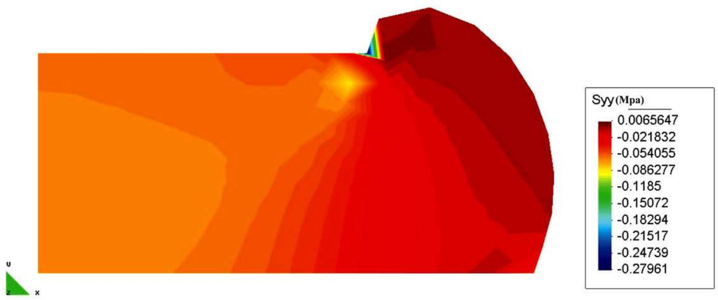

Figure 15: σ_{yy} profile (0,0016s^{-1}).

Mechanics of Solids in Brazil 2009, H.S. da Costa Mattos & Marcílio Alves (Editors)
Brazilian Society of Mechanical Sciences and Engineering, ISBN 978-85-85769-43-7

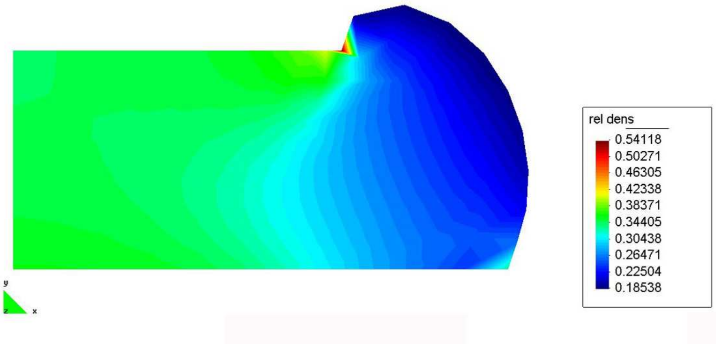

Figure 16: Relative density (0,0016 s^{-1} and 0,08 s^{-1}).

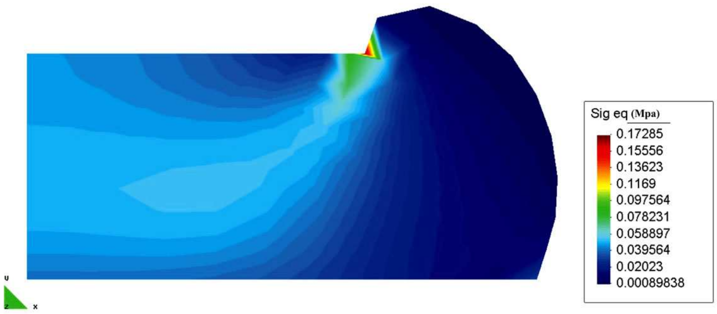

Figure 17: von Misses stress profile (0,08 s^{-1}).

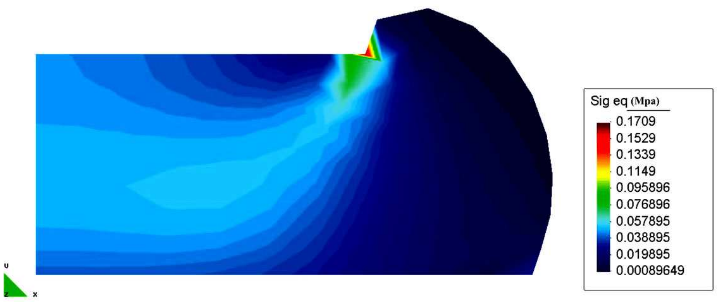

Figure 18: von Misses stress profile (0,0016s^{-1}).

Mechanics of Solids in Brazil 2009, H.S. da Costa Mattos & Marcílio Alves (Editors)
Brazilian Society of Mechanical Sciences and Engineering, ISBN 978-85-85769-43-7

10 Conclusions

The polymeric foam constitutive behavior is extremely complex on the micro structural scale. Cellular buckling under compression initiates a long stress plateau. Further compression causes stress build up due to foam consolidation.

A rate-dependent elasto-viscoplastic foam constitutive model, that features a single-surface yield criterion, has been developed. A non associated plastic flow law and the relative density dependence showed reasonable prediction for the responses of rigid polymeric foams under monotonic loading conditions.

The proposed polymeric foam model and the Galerkin-FEM algorithms was tested with a typical foam problem and has performed adequately. From the above considerations, one may conclude that the proposed model and numerical procedure showed to be adequate for the simulation of large strain behavior of polymeric crushable foams under monotonic loading conditions.

References

[1] Hallquist, J.O., *Theoritical Manual of LsDyna*. Livermore Software Technology Corporation, 1998.

[2] Hibbitt, H.D., *Models for crushable foams, version 6.5, ABAQUS theoretical Manual*. Karlsson and Sorensen Inc., 2000.

[3] Deshpande, V.S. & Fleck, N.A., Isotropic constitutive model for metallic foams. *J Mech Phys Solids*, **48**, pp. 1253–1276, 2000.

[4] Zhang, J., Kikuchi, N., Li, V.C., Yee, A.F. & Nusholtz, G.S., Constitutive modeling of polymeric foam material subjected to dynamic crash loading. *Int J Impact Engng*, **21(5)**, pp. 369–386, 1998.

[5] Zhang, J., Lin, Z., Wong, A., Kikuchi, N., Li, V.C., Yee, A.F. & Nusholtz, G.S., Constitutive modeling and material characterization of polymeric foams. *J Eng Mat Tech Trans ASME 119*, pp. 284–291, 1997.

[6] Gibson, L.J. & Ashby, M.F., *Cellular Solids: Structure and Properties*. Cambridge University Press, 1997.

[7] Gibson, L.J., Ashby, M.F., Zhang, J. & Triantafillou, T.C., Failure surfaces for cellular materials under multiaxial loads I: Modeling. *Int J Mech Sci*, **31(9)**, pp. 635–663, 1989.

[8] Gibson, L.J., Ashby, M.F., Zhang, J. & Triantafillou, T.C., Failure surfaces for cellular materials under multiaxial loads II: Comparisons of models with experiment. *Int J Mech Sci*, **31(9)**, pp. 665–678, 1989.

[9] Landro, L., Sala, G. & Olivieri, D., Deformation mechanisms and energy absorption of polystyrene foams for protective helmets. *Polymer Testing*, **21**, pp. 217–228, 2001.

[10] Roberts, A.P. & J., G.E., Elastic properties of model random three-dimensional open-cell solids. *Journal of the Mechanics and Physics of Solids*, **50**, pp. 33–55, 2002.

[11] Roberts, A.P. & J., G.E., Elastic moduli of model random three-dimensional closed-cell cellular solids. *Acta Materialia*, **49**, pp. 189–197, 2001.

[12] Chaboche, J.L. & Rousselier, G., On the plastic and viscoplastic constitutive equations – part I: rules developed with internal variable concept. *Journal of Pressure Vessel Technology*, **105**, pp. 153–158, 1983.

[13] Miller, A.K., Unified constitutive equations for creep and plasticity. *Elsevier applied Science*, 1987.

[14] Chaboche, J.L., Constitutive equations for cyclic plasticity and cyclic viscoplasticity. *Int J Plasticity*, **5**, pp. 247–302, 1989.

[15] Almroth, P., Hasselqvist, M., Simonsson, K. & Sjostrom, S., Viscoplastic-plastic modelling of in792. *Computational Materials Science*, **29**, pp. 437–445, 2004.

[16] Lemaitre, J.A., *A Course on Damage Mechanics*. Springer: Berlin, Germany, 1996.
[17] Hill, R., Aspects of invariance in solid mechanics. *Adv in Appl Mech*, **18**, pp. 1–75, 1978.
[18] Peric, D. & Owen, D.R.J., Finite-element applications to the nonlinear mechanics of solids. *Reports on Progress in Physics*, **61**, pp. 1495–1574, 1998.
[19] Weber, G. & Anand, L., Finite deformation constitutive equations and a time integration procedure for isotropic hyperelastic-viscoplastic solids. *Computer Methods in Applied Mechanics and Engineering*, **79**, pp. 173–202, 1990.
[20] G., H.A., S., H.O., H., L. & Ilstad, H., Validation of constitutive models applicable to aluminum foams. *International Journal of Mechanical Sciences*, 2001.
[21] A., G. & J., M.N., Impact deformation of rigid polymeric foams: experiments and FEA modeling. *International Journal of Impact Engineering*, **25**, pp. 767–786, 2001.

Mechanics of Solids in Brazil 2009, H.S. da Costa Mattos & Marcílio Alves (Editors)
Brazilian Society of Mechanical Sciences and Engineering, ISBN 978-85-85769-43-7